

Electronic Supplementary Information (ESI)

**Modeling of the cathodic and anodic polarization curves of
metals and alloys at an electronic level**

Yaolei Han,^{a,§} Guirong Su,^{b,§} Junjun Zhou,^b Ji-Chang Ren,^b Fei Xue,^a Huaiyu Hou,^b
Jinna Mei,^{a,*} Wei Liu,^{b,*} Tao Zhang^{c,*}

§ These authors contributed equally

* Corresponding authors

^a Suzhou Nuclear Power Research Institute, Suzhou 215004, China. Email:
meijinna@cgnpc.com.cn

^b Nano and Heterogeneous Materials Center, School of Materials Science and
Engineering, Nanjing University of Science and Technology, Nanjing 210094,
Jiangsu, China. Email: weiliu@njust.edu.cn.

^c Corrosion and Protection Division, Shenyang National Laboratory for Materials
Science, Northeastern University, Shenyang, 110819, China. Email:
zhangtao@mail.neu.edu.cn

Water splitting on the Cr-poor and Cr-rich surfaces. We further calculated the dissociative energy of H₂O molecule on the Fe-Cr alloys with the climbing image nudged elastic band (CI-NEB) method. In the dissociative process, water would be split into -H and -OH species, and then -OH further dissociates into -O and -H species. The structures of the initial state (IS), transition state (TS), final state (FS) and the energy barriers are shown in Figure S4 and Figure S5. Our results show that at the IS, the water molecule adsorbs at the top site on the substrate. While at the first step of the dissociative process the -H and -OH species are adsorbed at the hollow site. As shown in Figure S5, the reaction of the first step is exothermic by 0.7 eV and 0.89 eV for the Cr-poor system and Cr-rich system, respectively. In the TS1, the bond length between O and the stripped H is 1.37 Å (Cr-poor system) and 1.39 Å (Cr-rich system), which is obviously longer than that of the initial value (0.98 Å). The corresponding energy barrier in this process is 1.06 eV for the Cr-poor system and 1.08 eV for the Cr-rich system.

In the second reaction step of OH dissociation into O and H, the adsorption site of O remains unchanged, and the H atom forms a new Fe-H at the nearby hollow site. The reaction barrier of this step reduces to 0.72 eV and 0.84 eV for the Cr-poor and Cr-rich system, indicating that the first dissociation step of the Fe-Cr system become the reaction determination step in the whole process. According to the activation energies for TS1 of Cr-poor and Cr-rich system, it requires large energies to overcome the dissociative energy barriers. Hence, water molecules would not dissociate on the surfaces. We thus did not consider the dissociative adsorption mode in studying the adsorption of H₂O over the alloying surfaces.

Table S1. Calculated energy difference ΔE (eV) between systems of Cr-poor ($\text{Fe}_{23}\text{Cr}_1$) region with the Cr atom doping at 6 site and other sites.

| system | | site | | | | | | | |
|---|------------|-------|------|------|------|------|----------|------|------|
| | | 1 | 2 | 3 | 4 | 5 | 6 | 7 | 8 |
| Cr-poor region ($\text{Fe}_{23}\text{Cr}_1$) | ΔE | 0.02 | 0.86 | 0.83 | 0.90 | 0.85 | 0 | 1.02 | 0.91 |
| | ΔE | 0.60 | 0.59 | 0.59 | 0.60 | 0.59 | 0.60 | 0.60 | 0.60 |
| | ΔE | 0.002 | 0.91 | 1.02 | 0.93 | 0.72 | 0.02 | 0.87 | 0.02 |

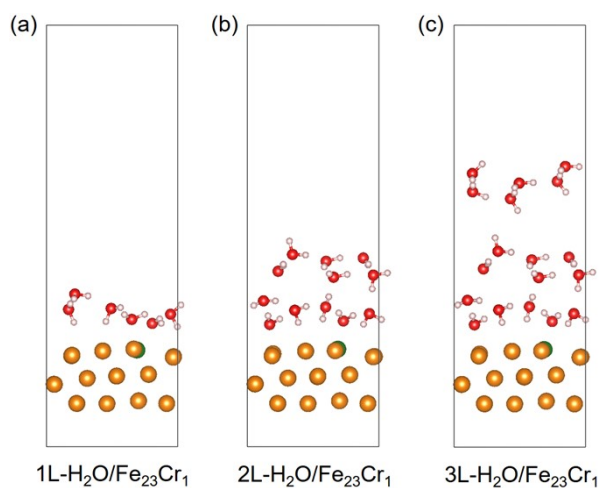


Figure S1. Optimized structures of one layer (a), two layers (b) and three layers (c) of water molecules on the $\text{Fe}_{23}\text{Cr}_1$ surface at the top site, calculated by the PBE+vdW method.

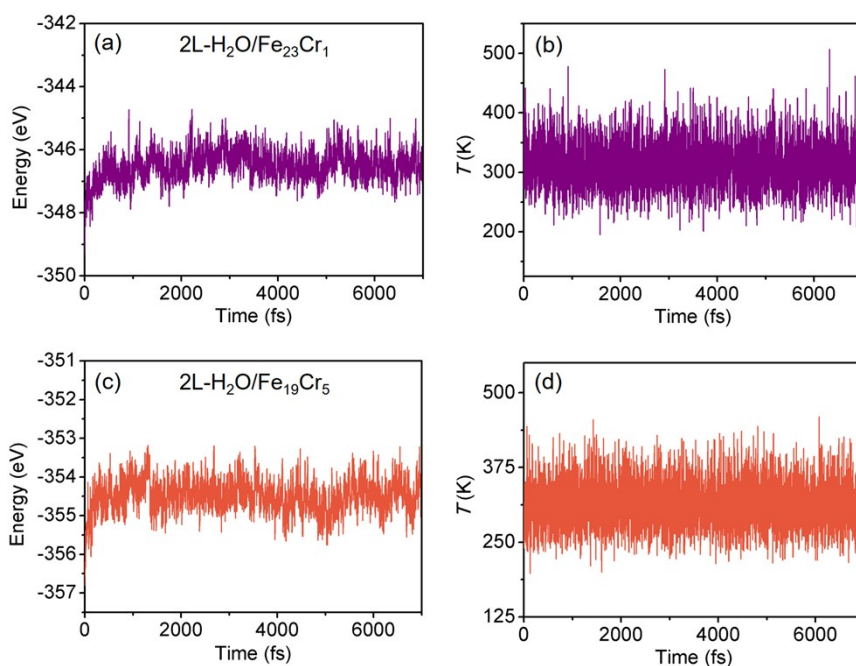


Figure S2. Energy changes of Cr-poor (a) and Cr-rich (c) system for 7 ps AIMD simulations at 300 K. The corresponding temperature changes during this process are shown in Figure (b) and (d), respectively.

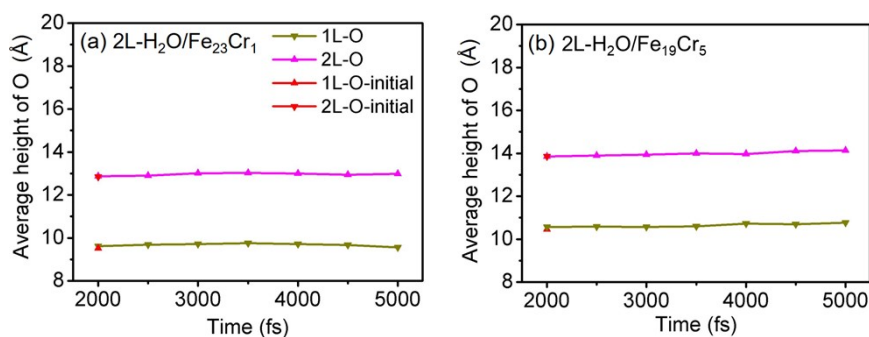


Figure S3. Average height of the first layer (1L-O) and second layer oxygen atoms (2L-O) of the Cr-poor (a) and Cr-rich (b) system along AIMD from 2 to 5 ps. The average height of 1L-O and 2L-O of the initial structure employed to perform the AIMD simulations are also shown as a reference.

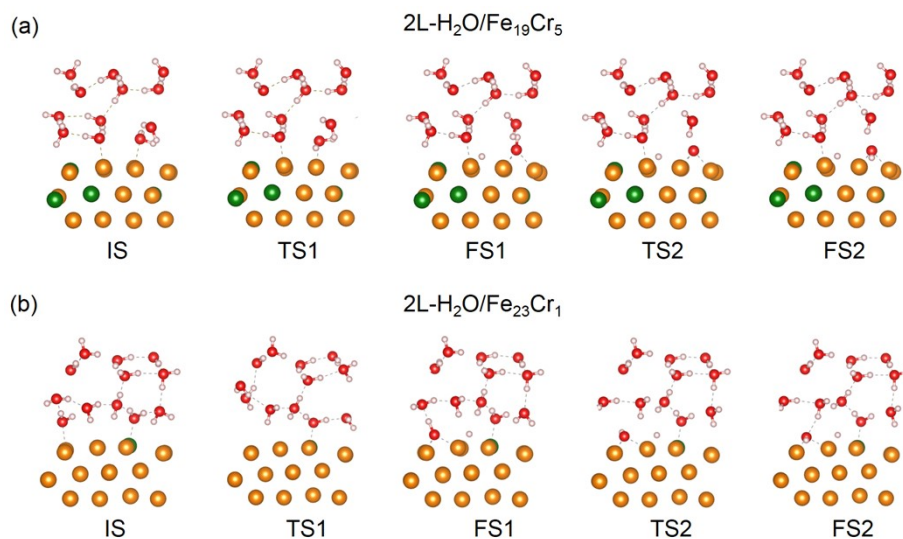


Figure S4. Optimized structures of the selected stationary points along the MEP for the water-splitting reaction on the (a) $\text{Fe}_{19}\text{Cr}_5$ and (b) $\text{Fe}_{23}\text{Cr}_1$ surfaces.

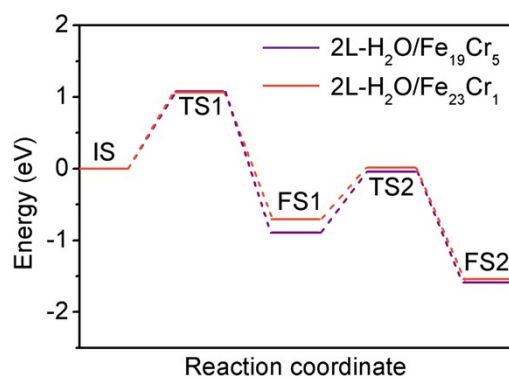


Figure S5. Schematic energy diagram for the dissociation of H_2O on $\text{Fe}_{19}\text{Cr}_5$ and $\text{Fe}_{23}\text{Cr}_1$ surfaces.